A study of Dynamic Properties of Recycled Granite Residual Soils with New Polymer SH

Bingxiang Yuan[1], Zihao Li[1], Zhilei Su[1], Wanying Wang[1*], Qingzi Luo[1], Zuqing Zhao[1], Minjie Chen[1]

[1]School of Civil and Transportation Engineering, Guangdong University of Technology, Guangzhou, 510006,China.

[1*]School of Civil and Transportation Engineering, Guangdong University of Technology, Guangzhou, 510006,China. 947210083@qq.com

Abstract: Improving and reusing construction waste soils is now more relevant in light of the need to decrease CO_2 emissions. In this paper, four contents of polymer SH (i.e., 0.0%, 3.0%, 3.5%, and 4.0%) were used to strengthen the granite residual soils, which is a kind of construction waste soils. Based on low-velocity impacts and employing scanning electron microscope (SEM) tests, this paper investigated the impact resistance of reinforced granite residual soils combined with polymer SH. Recycling waste granite residual soils can reduce the emissions of CO_2 generated during the transportation and disposal. The low-velocity impact tests were performed on specimens at three initial kinetic energy levels (i.e., 124.18J, 243.40J, and 402.36J) achieved by varying the drop height of the weights. The experimental results showed that the impact resistances of granite residual soils were enhanced significantly with a mixture of polymer SH, for which the increment reached the maximum with a 3.5% content of polymer SH. In addition, the microstructures of granite residual soils combined with four contents of polymer SH (i.e., 0.0%, 3.0%, 3.5%, and 4.0%) were

investigated using a Scanning Electron Microscope (SEM). The SEM images demonstrated that the interfaces of the granite residual soils particles became less distinct due to cementation with the increasing of the polymer SH content. With the optimal polymer SH content of 3.5%, the pore of granite residual soil was the smallest, resulting in a best enhancement of the impact resistance of the reinforced granite residual soil.

Keywords: granite residual soil; polymer SH; low-velocity impacts; SEM; impact resistance; initial kinetic energy

1. Introduction

With the acceleration of urbanization, dealing with construction waste has become a worrying problem. The construction waste soils have poor mechanical properties, which are not suitable for engineering construction. Therefore, transportation and disposal has become the preferred treatment method of dealing with such waste(Magnusson, Lundberg, Svedberg, & Knutsson, 2015). Construction waste soils are usually carried by heavy trucks and buried in a remote place. However, this solution could increase the building costs ($10-35/m^3) and might lead to negative influences on local and global environments. In the process of transportation, construction waste soils could generate a large amount of dust and lead to more serious smog pollution(Dong, Zhang, Long, Zhang, & Sun, 2019). Moreover, large and heavy vehicles carrying the construction waste soils could produce CO_2 and increase the greenhouse effect(Dong, Yu, & Pan, 2019). The CO_2 emissions would

also significantly increase the concentration of PM2.5 in the air;(Prah & Yun, 2018; Zheng, Ying, Wang, & Chen, 2018). Therefore, recycling waste soils can effectively decrease building costs and also reduce the air pollution. Improving the mechanical properties of construction waste soils could provide a new prospect for that recycling.

Whether soils can be used in engineering or not depends on its mechanical properties(Dai & Ng, 2014; C. Li, Zou, & Si-ga, 2019). The complex mechanical properties of soil depend on many factors, including particle size, permeability, soil types and water content(Chen, Xu, et al., 2019; Lu, Jing, Wang, & Xie, 2017; Wu, El Naggar, Abdlrahem, Mei, & Wang, 2017). Earlier studies demonstrated that granite residual soils couldn't be used in engineering because of high porosity and hydrophilicity, which were easy to disintegrate when subjected to water(W. Liu, Song, Huang, & Hu, 2019; W. P. Liu, Song, Luo, & Hu, 2020). Some scholars have conducted researches on the reinforcement mechanism of construction waste soil, which indicate that the addition of fiber and other substances is conducive to improving the strength of the soils(Nik Daud, Muhammed, & Kundiri, 2017; Y. X. Wang et al., 2018; Y. X. Wang et al., 2019; Y. X. Wang et al., 2017). Various enhancement methods have been developed to improve the mechanical properties of construction waste soils(Bilondi, Toufigh, & Toufigh, 2018; Sharaky, Mohamed, Elmashad, & Shredah, 2018; F. C. Wang, Ping, Zhou, & Kang, 2019). At present, it is relatively common to add glass fiber to construction waste soils to prevent cracks propagation(Saha & Bhowmik, 2018; Yeung et al., 2007). The reinforcement effect of

adding glass fiber is still not obvious because the brittle particles of construction waste soil weaken the connection between the soil and glass fiber. Different from glass fiber, the application of polymer SH can improve the mechanical properties of construction waste soil by cementing soil particles together. Existing research shows that the physicochemical interaction occurred between polymer SH and soil particles, by hydrogen bond, ion exchange, absorption of macromolecular, and flocculation(Y. M. Wang, Yang, Chen, & Han, 2005). The collapse resistance of soils after curing of polymer material SH was improved significantly(Wenwu, Qiyong, Hongwei, & Fei, 2017). As a new type of reinforcing material, the reinforcing effect of SH are still not well known, so this study selects the polymer SH developed by Lanzhou University as the curing agent.

The mechanical properties of soils also depend on different environmental conditions, different loading paths and different distribution forms(Chen, Liu, Ng, & Chen, 2019; Yang & Yuan, 2019). Existing studies demonstrate that when fluid infiltration, the soil looks mechanically stable concerning the shear strength parameters, for this is a soil with a mechanical behavior purely frictional(Pais, Gomes, & Falorca, 2012). However, the unsaturated shear strength of granite residual soil varies significantly with suction changes(P. Lin, Chen, & Wang, 2011). In particular, study of the dynamic properties of granite residual soils is still limited. Therefore, low-velocity impact was used to determine the impact resistance of reinforced granite residual soils in this paper.

Scholars employed different experimental methods to analyze the mechanical properties of soils(Gowthaman, Nakashima, & Kawasaki, 2018; Lu, Jing, Zhou, & Xie, 2017; Meng, Cui, & Li, 2020; Wu, Jiang, Huang, Mei, & Leo, 2017; Yuan et al., 2020). New techniques such as Particle Image Velocimetry (PIV) and Scanning Electron Microscope (SEM) were used to study the microstructure of soils(Sun & Tang, 2019; Yuan, Sun, et al., 2019; Yuan, Xiong, et al., 2019; Yuan, Xu, Wang, Chen, & Luo, 2017) .The main types of contact among the particles of granite residual soil include face-face, face-angle, face-edge, edge-edge, edge-angle and angle-angle contacts for particle size less than 0.2 mm. For the particle larger than 0.2 mm, new kind of contacts such as sphere-sphere, sphere-face, sphere-edge and sphere-angle would occur. Polymer SH would change the main types of contact among the particles. Observations of micro-structures by SEM allows us to better understand the reinforcing effect of SH used in the soil reinforcement(Bahmani, Farzadnia, Asadi, & Huat, 2016; Monatshebe, Mulaba-Bafubiandi, & Nyembwe, 2019). Li et al. interpreted the microstructural evolution of loess soils due to loading and wetting by the micrographs and variations in distributions of the pore morphology properties(P. Li, Xie, Pak, & Vanapalli, 2019). Lin et al. also found that microstructure plays an important role in controlling the deformational response to external stresses, resistance to shearing forces and electrochemical interactions between the particles and adjacent liquid or gas phase(B. T. Lin & Cerato, 2014).

This paper presents an experimental study of the dynamic mechanical properties

of a granite residual soil and explores the solidification properties and possible applications of the polymer material SH. Specifically, the influence of the content of the polymer SH on the properties of reinforced granite residual soil are studied using a low-velocity impacts test. SEM was also used to observe micro-structure and investigate the reinforcing effect of polymer SH as well as the effect of polymer SH on the micro-structure of granite residual soils.

2. Materials, apparatus and test procedures

2.1. Constituent Materials

The granite residual soils used in this study were yellowish brown or reddish brown and sampled from Guangdong Province (Fig. 1A). For this soils, the water content is 27%, wet density is 1.92 g/mm^3, oedometer modulus is 3MPa, friction angle is 20°and void ratio is 0.833. There were two reinforcement materials were used, one of which was Alkali resistant glass fiber (AR- glass fiber) produced by Taishan Fiberglss INC (Fig. 1B). Through the unconfined compression test results, the optimal dosage of glass fiber is 3% of the dry soil mass. The specification parameters of the AR- glass fiber are shown in Table 1.

Another reinforcement material was the new polymer SH. It is a non-toxic, nonpolluting, short gel and low viscosity curing material developed by Lanzhou University, P.R.C. (Fig. 1C). The concentration of polymer SH is 5%, and the polymer SH density is 1.27-1.31g/cm^3. Its main chain is a macromolecular chain linked by hydrophobic C-C bonds with hydrophilic groups (-OH) and carboxyl groups (-

COOH) on the chain. Three contents of polymer SH (i.e., 3.0%, 3.5%, and 4.0%) were added in the test specimens. 3.0%, 3.5%, and 4.0% are the possible optimal content obtained from unconfined compression test.

Table 1 Specification parameters of glass fiber

Model	Length	Fiber diameter	Density	Elastic Modulus	Tensile Strength
Cem-FIL62 chopped glass fiber	12-18mm	14μm	2.68g/cm^3	72GPa	1700MPa

Fig. 1 Material diagram: A) granite residual soil, B) AR- glass fiber, C) polymer SH

2.2. Preparation of Specimens

After crushing and sieving, the particle size of granite residual soil less than 1.18mm was selected for specimen preparation. Granite residual soils, purified water, polymer SH, AR-glass fiber are mixed in proportion and stirred well. The mass of dry soils m_d and water m_w required for specimen preparation corresponding to the required water content could be obtained from Equation 1 and Equation 2. The material contents for each sample are shown in Table 2. The prepared soil samples were poured into the mold and fixed in the compactor on the bottom plate. The soils were compacted by using a digital display automatic compactor.

$$m_{\mathrm{d}} = \frac{m_0}{1 + 0.01 w_0}$$

where m_d is the mass of dry soils; m_0 is the mass of the natural soils and w_0 is the natural water content.

$$m_w = \frac{m_0}{1 + 0.01 w_0} \times 0.01 \left(w' - w_0 \right)$$

where m_w is the water mass required for a specimen preparation; w' is the required water content of the specimen.

The low-velocity impact specimens were prepared according to the Chinese Standard GB/T 50123-2019 (Cai, Wang, et al., 2019), in which the specimens should be dried in the natural environment for 14 days. The geometrical dimensions of low-velocity impact specimens were 93 mm in diameter and 125 mm in height.

Table 2 Material Content of Sample

Test Specimen Number	Polymer SH	Water	Dry Soil	Fiberglass
LIT0025	0g	294g	2100g	0g
GF0045	0g	294g	2100g	63g
LIT3025	176.4g	117.6g	2100g	63g
LIT3035				
LIT3045				
LIT3525	205.8g	88.2g	2100g	63g
LIT3535				
LIT3545				
LIT4025	235.2g	58.8g	2100g	63g
LIT4035				
LIT4045				

2.3. Test procedures

2.3.1. Low-Velocity Impact tests

The low-velocity impact tests("Standard Test Method for Determination of the Impact Value (IV) of a Soil,") on the granite residual soil specimens were performed on an Instron Ceast 9350 drop-weight machine(Fig.2), in which a load cell and LVPT was used to measure the impact force and deformation response history respectively. The total mass of the drop weight was 39.739kg, and the initial kinetic energy was changed by different dropping height to achieve different initial impact velocities. In this study, three different initial impact velocities (i.e., 2.5m/s, 3.5m/s, and 4.5m/s) were pre-established, corresponding to three different initial kinetic energies (i.e., 124.18J, 243.40J, and 402.36J) respectively. The content ratio of polymer SH and loading conditions for the low velocity impact tests are shown in Table 3. It is noted that the abbreviation "LIT" in specimen number indicates the low-velocity impact test, and the abbreviation "GF" in specimen number indicates the soil only with glass fiber in low-velocity impact test. The first two digits represent the content of polymer SH, and the second two digits represent the loading rate.

The initial kinetic energy was determined by the weight of the drop hammer and the drop height. Therefore, the initial kinetic energy was changed by changing the drop height of the hammer head to achieve different initial impact velocities. According to kinetic energy theorem, the initial kinetic energy E_k was calculated by Equation 3.

$$E_k = \frac{1}{2}mv^2$$

where E_k is the initial kinetic energy, m is the total mass of the drop weight, v is initial falling velocity.

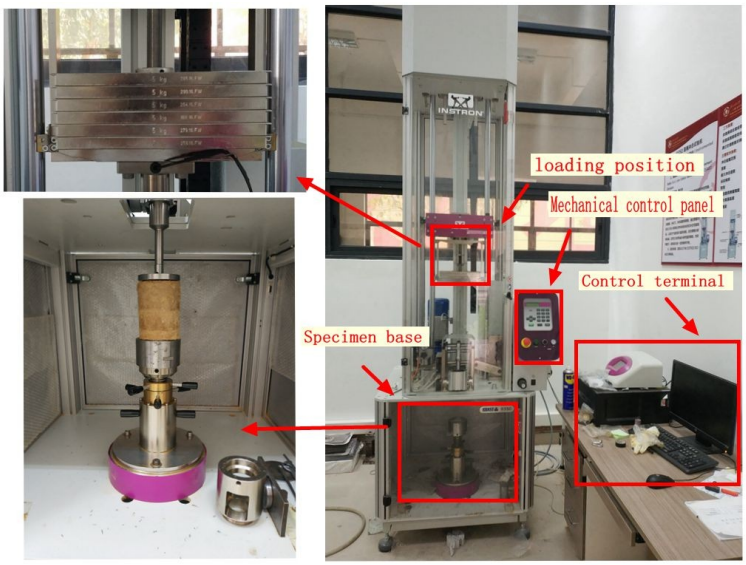

Fig. 2 Instron Ceast 9350 drop-weight machine

Table 3 Test Cases of Low Velocity Impact

Test Specimen number	Content of Polymer SH	Loading Rate	Initial kinetic energy
LIT0025	0.0%	2.5m/s	124.18J
LIT3025	3.0%	2.5m/s	124.18J
LIT3035	3.0%	3.5m/s	243.40J
LIT3045	3.0%	4.5m/s	402.36J
LIT3525	3.5%	2.5m/s	124.18J
LIT3535	3.5%	3.5m/s	243.40J
LIT3545	3.5%	4.5m/s	402.36J
LIT4025	4.0%	2.5m/s	124.18J
LIT4035	4.0%	3.5m/s	243.40J
LIT4045	4.0%	4.5m/s	402.36J
GF0045	0.0%	4.5m/s	402.36J

2.3.2. SEM Test

To capture the micro-structure of the reinforced granite residual soils and investigate the interaction reinforcing effect of the polymer SH and sand particles, SEM tests were conducted on reinforced granite residual soils with four contents of Polymer SH (i.e., 0.0%, 3.0%, 3.5%, and 4.0%). All test cases of SEM tests are shown in Table 4. The digits in the serial number indicates the content of the polymer SH.

Table 4 Test Cases of SEM Test

Test Specimen Number	Polymer SH Solution Content
SEM00	0.0%
SEM30	3.0%
SEM35	3.5%
SEM40	4.0%

3. Experimental Results

3.1. Experimental Results of Low-Velocity Impact Test

In the low-velocity impact tests, damage degree, the peak impact force and the compression deformation of granite residual soil combined with three contents of the polymer SH were investigated. Table 5 shows that the compressive deformation of LIT0025, LIT3025, LIT3525, and LIT4025 were 40.92, 5.80, 5.39, and 6.81mm, respectively. The compressive deformation of LIT3035, LIT3535, and LIT4035 were 8.99, 8.49, and 9.07mm, respectively. The compressive deformation of LIT3045, LIT3545, and LIT4045 were 12.14, 11.05, and 10.10mm, respectively. Fig. 3 shows that the damage degree of specimens under different initial kinetic energies. In Fig. 3A, the granite residual soil without polymer SH under the initial kinetic energy of

124.18J was completely broken. According to Figs. 3B and 4B, the reinforced granite residual soil with 3.5% contents of polymer SH under the initial kinetic energy of 124.18J only deforms vertically without obvious local damage. Figs. 3C and 4C show that under the initial kinetic energy of 243.40J, the compressive deformation of the reinforced granite residual soil combined with 3.5% contents of polymer SH is larger comparing with the that under the initial kinetic energy of 124.17J. In this case, the middle part of the specimen had a slight fracture while a slight radial expansion occurred at the bottom. When the initial kinetic energy increased to 402.36J, Figs. 3D and 4D show that the reinforced granite residual soil combined with 3.5% contents of polymer SH produced largest compressive deformation compared with the LIT3525 and the LIT3535. Compared with Figs. 3C and 4C, more significant fracture and radial expansion occurred in the middle part and bottom, respectively. It could be observed from Figs. 3B, 3C, 3D and 4 that all specimens could maintain suitable integrity although with different degrees of damage and fracture deformation.

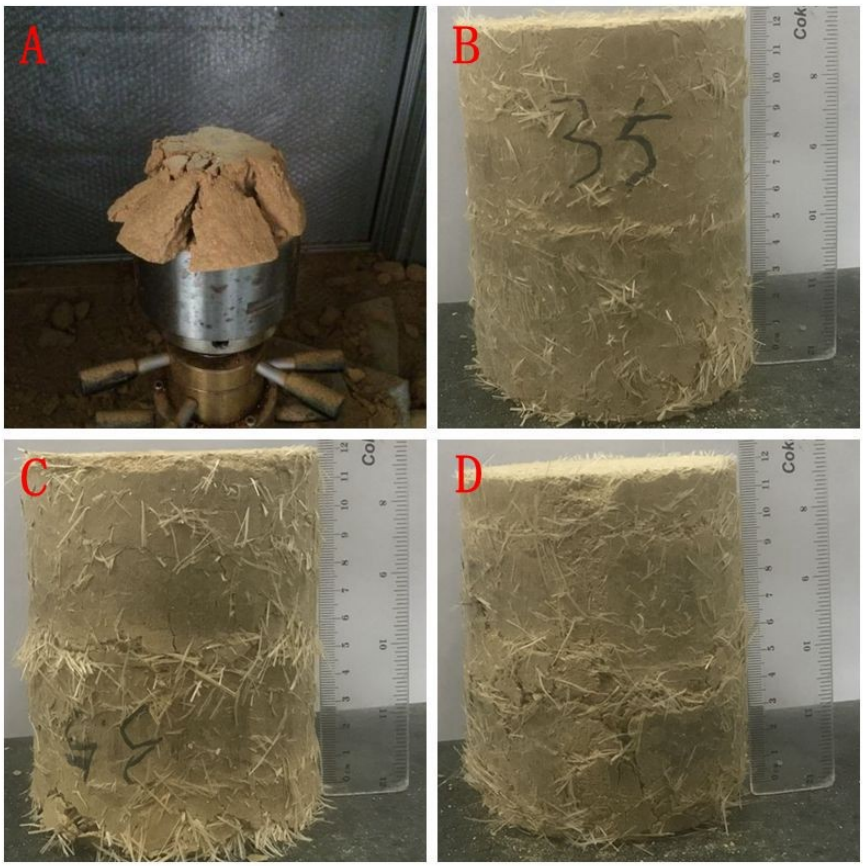

Fig. 3 Picture of test specimens under different initial kinetic energy; A) LIT0025,B) LIT3525,C) LIT3535,D) LIT3545

Table 5 shows that the peck impact force of the LIT0025, LIT3025, LIT3525, and LIT4025 were 9.87, 31.21, 37.36, 32.53kN and the final compressive deformation of the LIT0025, LIT3025, LIT3525, and LIT4025 were 40.92, 5.8, 5.39, 6.81mm, respectively. The peak impact force of the LIT3045, LIT3545, LIT4045, and GF0045 were 51.95, 60.02, 56.36, and 32.16kN and the final compressive deformation of the LIT3045, LIT3545, LIT4045, and GF0045 were 12.14, 11.05, 10.01, and 19.17mm, respectively. The peak impact force of LIT0025 was much smaller than that of the modified granite residual soil and the final compressive deformation of LIT0025 was much larger than that of the reinforced granite residual soils. The peak impact force of

40

235GF0045 was about half of that of LIT3045, LIT3545, and LIT4045 and the final 236compressive deformation of GF0045 was roughly double of that of LIT3045, 237LIT3545, and LIT4045. Overall, the results demonstrated that the impact resistance of 238granite residual soil modified by glass fiber and polymer SH was significantly 239improved from its unmodified condition or only with glass fiber.

240

241 Table 5 Experimental results of different proportions of polymer SH under different initial kinetic
242 energies

Test Specimen Number	Peak Impact Force(kN)	Final Compression Deformation(mm)	Time(ms)
LIT0025	9.87	40.92	22.97
LIT3025	31.21	5.80	7.22
LIT3035	42.91	8.99	7.16
LIT3045	51.95	12.14	7.60
LIT3525	37.36	5.39	6.31
LIT3535	42.51	8.49	7.19
LIT3545	60.02	11.05	6.55
LIT4025	32.53	6.81	7.39
LIT4035	43.08	9.07	7.09
LIT4045	56.36	10.10	7.11
GF0045	32.16	19.17	11.30

243

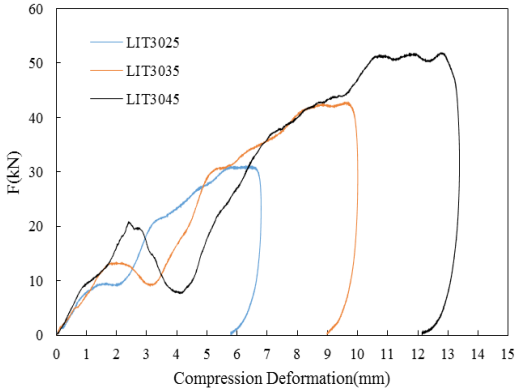

(A)3.0% concentration (B)3.5% concentration

41

42

(C)4.0% concentration

Fig. 4 Relationship between compressive deformation and impact force of the same concentration under different initial kinetic energies

Fig. 4 showed the relationship between compressive deformation and impact force at different velocity, in which two phenomena were presented. On the one hand, with the increase of initial kinetic energy, compressive deformation and impact force of the specimens with the same concentration increased. On the other hand, the maximum point of the curve moved to the right, which meant compressive deformation corresponding with maximum impact force increased. Particularly, in Fig. 4(A) and 4(B), the horizontal distance between the maximum points of the three curves is about 3mm, and it is about 2mm in Fig. 4(C). In other words, Comparing with 3.0% and 3.5% concentration, as the initial kinetic energy of the specimen with 4.0% concentration increased, the compressive deformation increment corresponding to the maximum load was smaller. It was speculated that the increase in the polymer SH content reduced the pores. After the specimen was subjected to an impact load, pore compression and rearrangement of soil particles would occur. After pore compressive and rearrangement of soil particles, the pores would be further subjected to the impact load. The reduction reduced the compressive deformation during the pore extrusion and particle recombination stages.

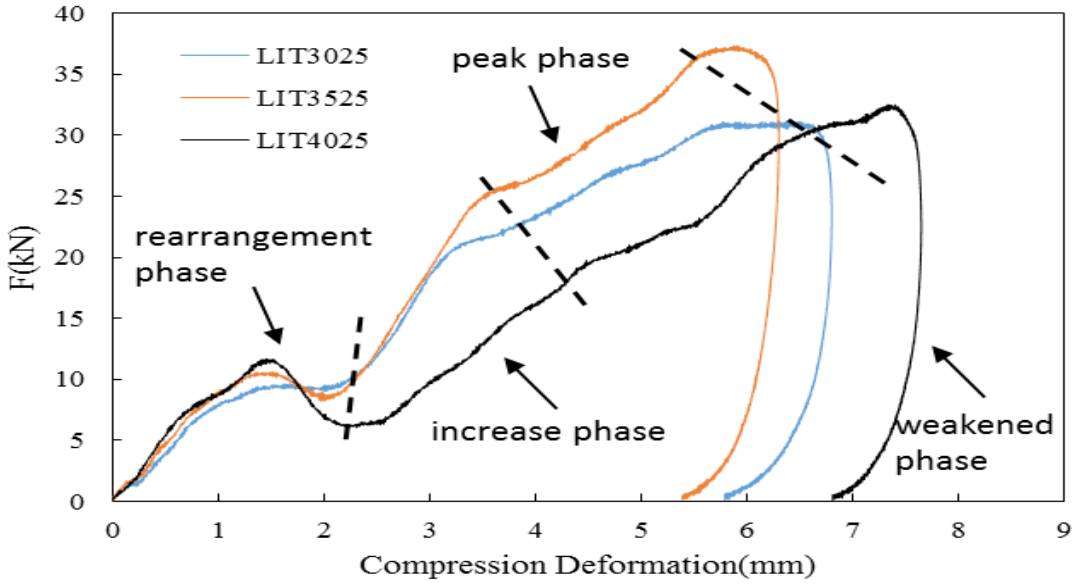

Fig. 5 Relationship between compressive deformation and impact force of 124.18J

Figs. 5-7 are the impact force-compassion deformation, compassion deformation-time, and impact force-time curves of specimens with different polymer SH contents in low-velocity impact tests, respectively. In each impact test, the compassion deformation increased with the increase of the impact force and decreased with the decrease of the impact force. Granite residual soil compressed pores and rearranged particles after impact loading. Therefore, these impact force-compassion deformation curves went through four phases, including rearrangement phase, increase phase, peak phase and weakened phase.

The peak impact force of LIT3025, LIT3525, and LIT4025 were 31.21kN, 37.36kN, and 32.53kN and the compressive deformation of LIT3025, LIT3525, and LIT4025 were 5.80mm, 5.39mm, and 6.81mm, respectively. As shown in Fig. 6, under the condition of the initial kinetic energy of 124.18J, the content of polymer SH in the reinforced granite residual soils would affect the impact resistance and compressive deformation of the specimens. Under the same compressive deformation, the peak impact force of the LIT3525 was bigger than that of the LIT3025 and

LIT4025 in increase phase, and the final compressive deformation of the LIT3525 was the smallest, which was 5.3mm. The slope of LIT3525 curve was larger than that of LIT3025 and LIT025 in increase phase. The slope of the curve is the ratio of force to deformation, the magnitude of the slope can reflect the change of its impact resistance. The test results demonstrated that LIT3525, that is, the reinforced granite residual soils combined with 3.5% polymer SH, had the best impact resistance under the initial kinetic energy of 124.18J.

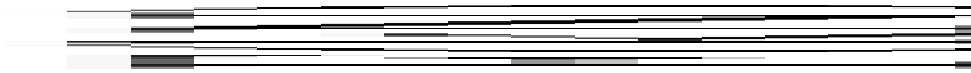

Fig. 6 Relationship between compressive deformation and impact force of 243.40J

Fig. 6 shows that unlike the initial kinetic energy of 124J, when the initial kinetic energy of 243.40J, the impact resistance curves of the reinforced granite residual soil combined with different content of polymer SH are similar, and the curves of the LIT3035 and LIT4035 almost coincide because when the initial kinetic energy was 124J, the initial kinetic energy is relatively small, resulting in the uneven surface of

the test piece will produce a difference in test results. The peak impact force of the three contents of polymer SH is similar, but the final compression deformation of the LIT3535 is smaller than that of the LIT3035 and LIT4035 and the slope of LIT3535 curve was slightly larger than that of LIT3035 and LIT035 in increase phase.. The test results demonstrate that, although the impact bearing capacities of all specimens are similar, the final compressive deformation and the curve slope in increase phase of the LIT3535 were better than the LIT3035 and LIT4035. What this means is that, under low initial kinetic energy of 243.40J, the impact resistance of the reinforced granite residual soil with a 3.5% content of polymer SH is slightly better than that of the other two contents.

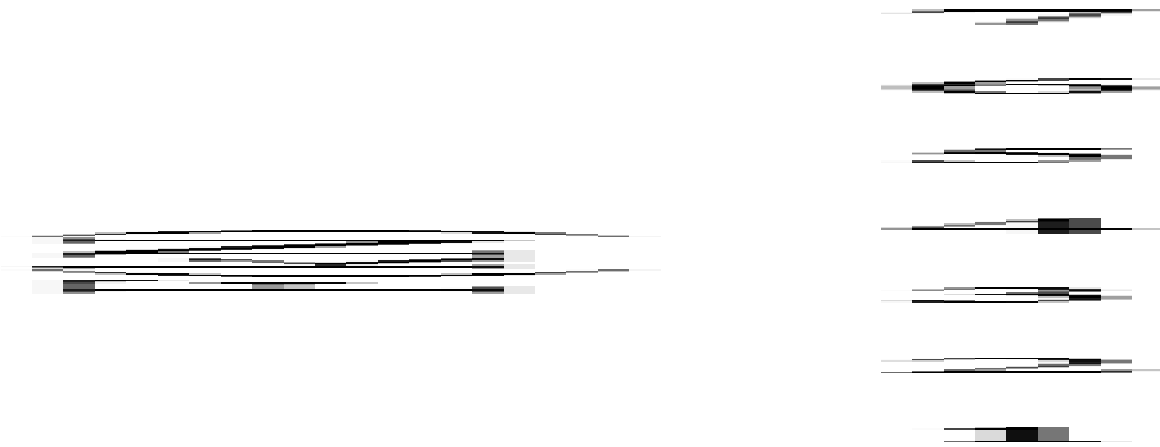

Fig. 7 Relationship between compressive deformation and impact force of 402.36J

In Fig. 7, under the initial kinetic energy of 402.36J, the impact force-compressive deformation curves of the reinforced granite residual soil combined with

different content of polymer SH have obvious differences because the initial kinetic energy was large enough to distinguish the impact resistance of different SH. The peak impact force and the curve slope in increase phase of LIT3545 were larger than that of the LIT3045 and LIT4045, but the final compressive deformation was smallest of the LIT4045. Unlike the case where initial kinetic energy was 124.18 and 243.40J, the possible reason why the final compressive deformation was smallest was that the pores of LIT4045 were less than those of LIT3045 and LIT3545. The large initial kinetic energy causes the pores of LIT3045 and LIT3545 to be compressed as much as possible during the rearrangement phase and the compressive deformation is larger than LIT4045. The test results demonstrate that the compressive deformation of the reinforced granite residual soil combined with 4.0% content of polymer SH was smaller than the other two contents. However, the peak impact force and the curve slope of the reinforced granite residual soil combined with 3.5% content of polymer SH is the largest. Therefore, the impact resistance of the reinforced granite residual soil combined with 3.5% content of polymer SH is the best under the initial kinetic energy of 402.36J.

The analysis of different initial kinetic energies in the impact tests demonstrate that the damage degree of the test specimen become more and more obvious with the increase of initial kinetic energy. Compared with the granite residual soil without polymer SH, the impact resistance of the reinforced residual soil combined with each content of the polymer SH is remarkably improved. According to the comparison of

the compressive capacity, impact bearing capacity of the reinforced granite residual soil combined with each content of the polymer SH, the reinforced residual soil combined with the 3.5% content of polymer SH has the best impact resistance under each initial kinetic energy. The 3.5% content of polymer SH is a relatively optimal proportion for the reinforced granite residual soil.

3.2. Experimental Results of SEM Test

In this part of the study, Glass fibers were difficult to observe because the polymer SH made the soil wrapped on the glass fiber. Therefore, SEM was mainly used to observe the microstructure of reinforced granite residual soil with polymer SH and further study the reinforcing effect of polymer SH. The SEM experiments use the range of 7.6-7.8 mm resolution and 100, 1,000, and 7,000 magnification. The white highlight in the picture is the soil particles with higher moisture.

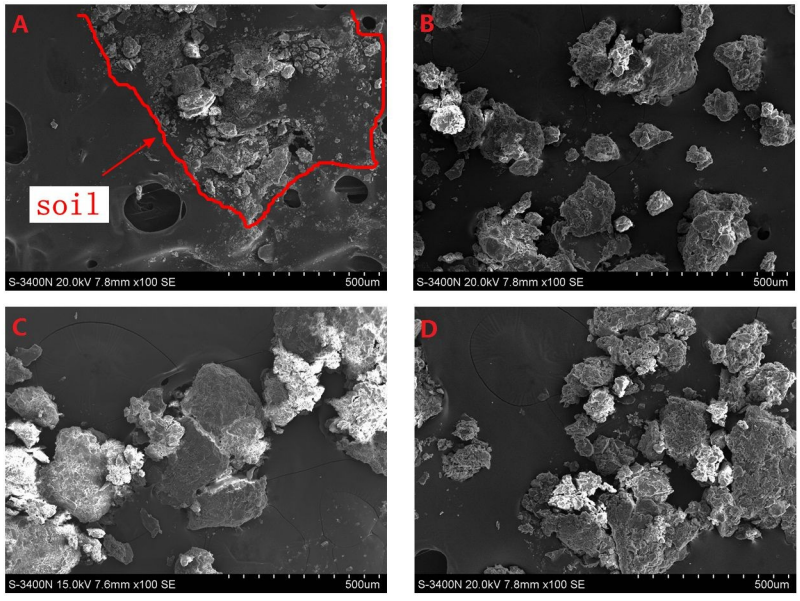

Fig. 8 Microstructure diagram at 100 magnification: A)SEM00, B)SEM30, C)SEM35, D)SEM40

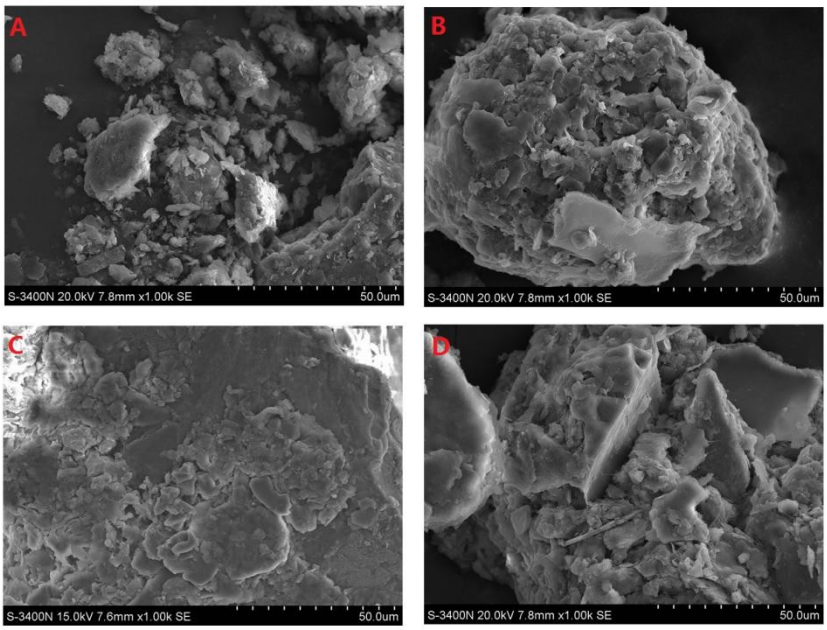

Fig. 9 Microstructure diagram at 1,000 magnification: A)SEM00, B)SEM30, C)SEM35, D)SEM40

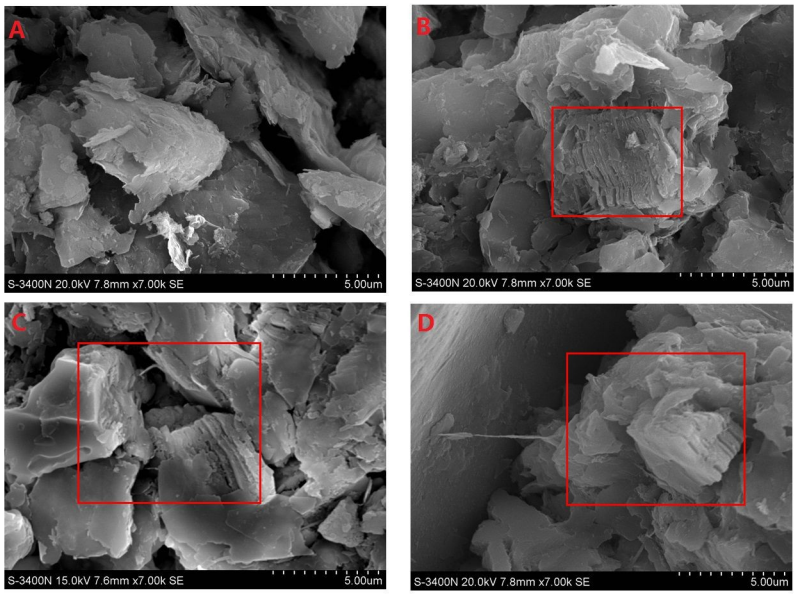

Fig. 10 Microstructure diagram at 7,000 magnification: A)SEM00, B)SEM30, C)SEM35, D)SEM40

Table 6 Pore and soil area, and its ratio

Test Specimen Number	Pore Area(mm^2)	Soil Area(mm^2)	Ratio of Pore to Soil Area
SEM00	577.5904	2351.093	25%
SEM30	1209.969	6566.356	18%
SEM35	654.0535	5002.97	13%
SEM40	704.0094	7580.767	9%

Table 6 is the data obtained by analyzing the area of soil and pores and their ratio in the scanning electron microscope image with 1,000 times magnification by software. It can be seen from Table 6 that with the increase of polymer SH, because the polymer SH cements the soil together, the soil particles increase and the porosity decreases, which verifies that the porosity decreases in the drop weight test.

As shown in Fig. 8, under the same magnification, the particle sizes of SEM30, SEM35, and SEM40 are larger than the particle sizes of SEM00 at the magnification of 0.1 K, some particles in the picture are bright white due to high water content. In order to observe the particle structure, the magnification increases from 0.1 K to 1 K. Fig. 9 shows that at the magnification of 1 K, the particles of SEM00 are relatively separate, and the Variation of particle size is large. By contrast, the particles of SEM30, SEM35, and SEM40 are mostly aggregated. With the increasing of magnification from 1 K to 7 K, observation of bonding between the particles could be helpful to further study the reinforcing effect of polymer SH. In the rectangular frame in Fig. 10B, at the magnification of 7K, the boundary between the aggregated particles of SEM30 is clear, while the boundary between the aggregated particles of SEM35 are blurred, and the boundary between the aggregated particles of SEM40 is difficult to distinguish. As can be seen from Figs. 8-10, with the increasing of the content of the polymer SH, the degree of particle aggregation become higher cause the particle size to become larger, fewer pores, and the strength of the particles to decreased. In addition, aggregated particle size affects the main types of contact

between particles. The main contact types of SEM00 are face-angle, edge-angle, and angle-angle contacts because the particles of SEM00 are small and irregular in shape. In contrast, the main contact types of SEM30 are face-face, face-edge, and edge-edge. The secondary contact types of SEM30 are ace-edge, edge-angle because fewer small particles are interspersed among larger particles. The main contact types of SEM35 and SEM40 are face-face, face-angle, and face-edge contacts. Different from SEM35, the degree of aggregation of SEM40 particles is higher, resulting in the presence of bulges on the surface of large particles. The bulges on the surface of large particles were more fragile, leading to the decrease in strength. The SEM results verify that as the SH concentration increases, the particle size increases and the pores decrease, so compressive deformation of LIT4045 was the smallest in the rearrangement phase, and final compressive deformation of LIT4045 was the smallest. However, the larger aggregated particles of LIT4045 resulted in lower particle strength, so the curve slope of LIT4045 decreased in the increase phase, and the peak impact force of LIT4045 was less than B. Therefore, the impact resistance of reinforced granite residual soils combined with 4.0% content of polymer SH is slightly less than that of the 3.5% content. Combined with the low-velocity impact test, the SEM results further confirm that reinforced granite residual soil combined with 3.5% content of polymer SH has better impact resistance.

4. Conclusion

In this paper, the impact resistance of reinforced granite residual soils combined

with the polymer SH and glass fiber was investigated using low-velocity impact tests and SEM tests. Moreover, the reinforcement effect of polymer SH were discussed.

In the low-velocity impact tests, according to the comparison of peak impact force, compressive deformation, and curve slope of the reinforced residual soils with different contents of polymer SH, the impact resistance of reinforced granite residual soil with 3.5% content of polymer SH was better than that of the 3.0% and 4.0% contents.

The SEM results further confirm that reinforced granite residual soil combined with 3.5% content of polymer SH has better impact resistance. With the increasing of the content of the polymer SH, the degree of particle aggregation become higher cause the particle size to become larger, fewer pores, and the strength of the particles to decreased. In addition, the main contact types between particles changed with the degree of particle aggregation. When the content of SH exceeded 3.5%, the impact resistance of reinforced granite residual soils with polymer SH will be reduced.

Compared to the granite residual soils without polymer SH or only with glass fiber, the impact resistance of reinforced granite residual soils with polymer SH was significantly improved. In the actual foundation pit engineering and slope reinforcement, reutilization of granite residual soil or Reinforced granite residual soil combined with polymer SH can improve economic benefits and decrease building cost. Consequently, the recycling construction waste soil can replace the concrete to reduce the pollution to the environment.

Acknowledgement

The authors would gratefully like to acknowledge the support provided by the National Natural Science Foundation of China (Nos. 51978177, 51809050, and 41741902288), by the Science and Technology Plan Project of Guangdong Provincial Department of Transportation (2017-02-018), by the Guangdong Natural Science Foundation (No. 2018A030313839). The editorial help from Professor Galen Leonhardy of Black Hawk College is also greatly appreciated.

References

Bahmani, S. H., Farzadnia, N., Asadi, A., & Huat, B. B. K. (2016). The effect of size and replacement content of nanosilica on strength development of cement treated residual soil. *Construction and Building Materials, 118*, 294-306. Retrieved from <Go to ISI>://WOS:000378181800031. doi:10.1016/j.conbuildmat.2016.05.075

Bilondi, M. P., Toufigh, M. M., & Toufigh, V. (2018). Experimental investigation of using a recycled glass powder-based geopolymer to improve the mechanical behavior of clay soils. *Construction and Building Materials, 170*, 302-313. Retrieved from <Go to ISI>://WOS:000431158200029. doi:10.1016/j.conbuildmat.2018.03.049

Chen, R., Liu, J., Ng, C. W. W., & Chen, Z. K. (2019). Influence of Slope Angle on Water Flow in a Three-Layer Capillary Barrier Soil Cover under Heavy Rainfall. *Soil Science Society of America Journal, 83*(6), 1637-1647. Retrieved from <Go to ISI>://WOS:000502983600004. doi:10.2136/sssaj2019.05.0135

Chen, R., Xu, T., Zhao, Y. R., Deng, G., Qiao, J., & Zhou, S. (2019). Effects of net normal stress on hydro-mechanical behaviour of a kaolinite clay soil under different suction paths. *Environmental Earth Sciences, 78*(24), 15. Retrieved from <Go to ISI>://WOS:000511854300030. doi:10.1007/s12665-019-8698-x

Dai, Q. L., & Ng, K. (2014). 2D cohesive zone modeling of crack development in cementitious digital samples with microstructure characterization. *Construction and Building Materials, 54*, 584-595. Retrieved from <Go to ISI>://WOS:000333885000064. doi:10.1016/j.conbuildmat.2013.12.095

Dong, F., Yu, B. L., & Pan, Y. L. (2019). Examining the synergistic effect of CO2 emissions on PM2.5 emissions reduction: Evidence from China. *Journal of Cleaner*

Production, 223, 759-771. Retrieved from <Go to ISI>://WOS:000466253100063. doi:10.1016/j.jclepro.2019.03.152

Dong, F., Zhang, S. N., Long, R. Y., Zhang, X. Y., & Sun, Z. Y. (2019). Determinants of haze pollution: An analysis from the perspective of spatiotemporal heterogeneity. *Journal of Cleaner Production, 222*, 768-783. Retrieved from <Go to ISI>://WOS:000466249500067. doi:10.1016/j.jclepro.2019.03.105

Gowthaman, S., Nakashima, K., & Kawasaki, S. (2018). A State-of-the-Art Review on Soil Reinforcement Technology Using Natural Plant Fiber Materials: Past Findings, Present Trends and Future Directions. *Materials, 11*(4), 23. Retrieved from <Go to ISI>://WOS:000434710200095. doi:10.3390/ma11040553

Li, C., Zou, J. F., & Si-ga, A. (2019). Closed-Form Solution for Undrained Cavity Expansion in Anisotropic Soil Mass Based on Spatially Mobilized Plane Failure Criterion. *International Journal of Geomechanics, 19*(7), 13. Retrieved from <Go to ISI>://WOS:000468408200022. doi:10.1061/(asce)gm.1943-5622.0001458

Li, P., Xie, W. L., Pak, R. Y. S., & Vanapalli, S. K. (2019). Microstructural evolution of loess soils from the Loess Plateau of China. *Catena, 173*, 276-288. Retrieved from <Go to ISI>://WOS:000452814300027. doi:10.1016/j.catena.2018.10.006

Lin, B. T., & Cerato, A. B. (2014). Applications of SEM and ESEM in Microstructural Investigation of Shale-Weathered Expansive Soils along Swelling-Shrinkage Cycles. *Engineering Geology, 177*, 66-74. Retrieved from <Go to ISI>://WOS:000339039400007. doi:10.1016/j.enggeo.2014.05.006

Lin, P., Chen, H., & Wang, Y. (2011). *Behavior of the Unsaturated Granite Residual Soil and Its Effects on Embankment Project.* Paper presented at the GeoHunan International Conference 2011.

Liu, W., Song, X., Huang, F., & Hu, L. (2019). Experimental study on the disintegration of granite residual soil under the combined influence of wetting-drying cycles and acid rain. *Geomatics Natural Hazards & Risk, 10*(1), 1912-1927. Retrieved from <Go to ISI>://WOS:000482919900001. doi:10.1080/19475705.2019.1651407

Liu, W. P., Song, X. Q., Luo, J., & Hu, L. N. (2020). The processes and mechanisms of collapsing erosion for granite residual soil in southern China. *Journal of Soils and Sediments, 20*(2), 992-1002. Retrieved from <Go to ISI>://WOS:000492327300001. doi:10.1007/s11368-019-02467-4

Lu, M. M., Jing, H. W., Wang, B., & Xie, K. H. (2017). Consolidation of composite ground improved by granular columns with medium and high replacement ratio. *Soils and Foundations, 57*(6), 1088-1095. Retrieved from <Go to ISI>://WOS:000418424000015. doi:10.1016/j.sandf.2017.08.033

Lu, M. M., Jing, H. W., Zhou, Y., & Xie, K. H. (2017). General Analytical Model for Consolidation of Stone Column-Reinforced Ground and Combined Composite Ground. *International Journal of Geomechanics, 17*(6), 18. Retrieved from <Go to ISI>://WOS:000399425700018. doi:10.1061/(asce)gm.1943-5622.0000836

Magnusson, S., Lundberg, K., Svedberg, B., & Knutsson, S. (2015). Sustainable management of excavated soil and rock in urban areas - A literature review. *Journal of*

Cleaner Production, 93, 18-25. Retrieved from <Go to ISI>://WOS:000353095100003. doi:10.1016/j.jclepro.2015.01.010

Meng, K., Cui, C. Y., & Li, H. J. (2020). An Ontology Framework for Pile Integrity Evaluation Based on Analytical Methodology. *Ieee Access, 8*, 72158-72168. Retrieved from <Go to ISI>://WOS:000530816700001. doi:10.1109/access.2020.2986229

Monatshebe, T., Mulaba-Bafubiandi, A. F., & Nyembwe, D. K. (2019). Mechanical properties and mineralogy of artisanal clay bricks manufactured in Dididi, Limpopo, South Africa. *Construction and Building Materials, 225*, 972-982. Retrieved from <Go to ISI>://WOS:000488305700082. doi:10.1016/j.conbuildmat.2019.07.247

Nik Daud, N., Muhammed, A., & Kundiri, A. (2017). Hydraulic Conductivity of Compacted Granite Residual Soil Mixed with Palm Oil Fuel Ash in Landfill Application. *Geotechnical and Geological Engineering, 35*(5), 1967-1976. Retrieved from <Go to ISI>://WOS:000411115900005. doi:10.1007/s10706-017-0220-1

Pais, L. J. A., Gomes, L. M. F., & Falorca, I. M. C. F. G. (2012). *Shear Strength and Permeability of Granite Residual Soil Contaminated with Urban Solid Waste Leachate.* Paper presented at the Geocongress.

Prah, B., & Yun, R. (2018). CO2 hydrate slurry transportation in carbon capture and storage. *Applied Thermal Engineering, 128*, 653-661. Retrieved from <Go to ISI>://WOS:000414884700063. doi:10.1016/j.applthermaleng.2017.09.053

Saha, H. S., & Bhowmik, D. (2018). Effect of Glass Fiber on Shear Strength of Soil. *Key Engineering Materials, 775*, 603-609.

Sharaky, A. M., Mohamed, N. S., Elmashad, M. E., & Shredah, N. M. (2018). Application of microbial biocementation to improve the physico-mechanical properties of sandy soil. *Construction and Building Materials, 190*, 861-869. Retrieved from <Go to ISI>://WOS:000451104900074. doi:10.1016/j.conbuildmat.2018.09.159

Standard Test Method for Determination of the Impact Value (IV) of a Soil. *Astm*.

Sun, Y. L., & Tang, L. S. (2019). Use of X-ray computed tomography to study structures and particle contacts of granite residual soil. *Journal of Central South University, 26*(4), 938-954. Retrieved from <Go to ISI>://WOS:000466892300016. doi:10.1007/s11771-019-4062-2

Wang, F. C., Ping, X. W., Zhou, J. H., & Kang, T. B. (2019). Effects of crumb rubber on the frost resistance of cement-soil. *Construction and Building Materials, 223*, 120-132. Retrieved from <Go to ISI>://WOS:000487569100011. doi:10.1016/j.conbuildmat.2019.06.208

Wang, Y. M., Yang, Z. C., Chen, W. W., & Han, W. F. (2005). STRENGTH CHARACTERISTICS AND MECHANISM OF LOESS SOLIDIFIED WITH NEW POLYMER MATERIAL SH. *Chinese Journal of Rock Mechanics and Engineering, 24*(14), 2554-2559.

Wang, Y. X., Guo, P. P., Dai, F., Li, X., Zhao, Y. L., & Liu, Y. (2018). Behavior and Modeling of Fiber-Reinforced Clay under Triaxial Compression by Combining the Superposition Method with the Energy-Based Homogenization Technique. *International Journal of Geomechanics, 18*(12), 22. Retrieved from <Go to ISI>://WOS:000447361300020. doi:10.1061/(asce)gm.1943-5622.0001313

Wang, Y. X., Guo, P. P., Li, X., Lin, H., Liu, Y., & Yuan, H. P. (2019). Behavior of Fiber-Reinforced and Lime-Stabilized Clayey Soil in Triaxial Tests. *Applied Sciences-Basel, 9*(5), 15. Retrieved from <Go to ISI>://WOS:000462504400087. doi:10.3390/app9050900

Wang, Y. X., Guo, P. P., Ren, W. X., Yuan, B. X., Yuan, H. P., Zhao, Y. L., . . . Cao, P. (2017). Laboratory Investigation on Strength Characteristics of Expansive Soil Treated with Jute Fiber Reinforcement. *International Journal of Geomechanics, 17*(11), 12. Retrieved from <Go to ISI>://WOS:000417684800010. doi:10.1061/(asce)gm.1943-5622.0000998

Wenwu, C., Qiyong, Z., Hongwei, L., & Fei, G. (2017). REINFORCING EFFECT OF RELIC SOIL SITES PENETRATED WITH HIGH POLYMER MATERIAL SH. *Journal of Engineering Geology*.

Wu, W. B., El Naggar, M. H., Abdlrahem, M., Mei, G. X., & Wang, K. H. (2017). New interaction model for vertical dynamic response of pipe piles considering soil plug effect. *Canadian Geotechnical Journal, 54*(7), 987-1001. Retrieved from <Go to ISI>://WOS:000404459000008. doi:10.1139/cgj-2016-0309

Wu, W. B., Jiang, G. S., Huang, S. G., Mei, G. X., & Leo, C. J. (2017). A new analytical model to study the influence of weld on the vertical dynamic response of prestressed pipe pile. *International Journal for Numerical and Analytical Methods in Geomechanics, 41*(10), 1247-1266. Retrieved from <Go to ISI>://WOS:000403000000002. doi:10.1002/nag.2670

Yang, B. B., & Yuan, J. H. (2019). Influence of Soda Content on Desiccation Cracks in Clayey Soils. *Soil Science Society of America Journal, 83*(4), 1054-1061. Retrieved from <Go to ISI>://WOS:000484542400009. doi:10.2136/sssaj2018.05.0204

Yeung, A. T., Cheng, Y. M., Tham, L. G., Au, A. S. K., So, S. T. C., & Choi, Y. K. (2007). Field evaluation of a glass-fiber soil reinforcement system. *Journal of Performance of Constructed Facilities, 21*(1), 26-34. Retrieved from <Go to ISI>://WOS:000243573100005. doi:10.1061/(asce)0887-3828(2007)21:1(26)

Yuan, B. X., Sun, M., Wang, Y. X., Zhai, L. H., Luo, Q. Z., & Zhang, X. Q. (2019). Full 3D Displacement Measuring System for 3D Displacement Field of Soil around a Laterally Loaded Pile in Transparent Soil. *International Journal of Geomechanics, 19*(5), 8. Retrieved from <Go to ISI>://WOS:000462449600017. doi:10.1061/(asce)gm.1943-5622.0001409

Yuan, B. X., Sun, M., Xiong, L., Luo, Q. Z., Pradhan, S. P., & Li, H. Z. (2020). Investigation of 3D deformation of transparent soil around a laterally loaded pile based on a hydraulic gradient model test. *Journal of Building Engineering, 28*, 5. Retrieved from <Go to ISI>://WOS:000513823200056. doi:10.1016/j.jobe.2019.101024

Yuan, B. X., Xiong, L., Zhai, L. H., Zhou, Y. F., Chen, G. F., Gong, X., & Zhang, W. (2019). Transparent Synthetic Soil and Its Application in Modeling of Soil-Structure Interaction Using Optical System. *Frontiers in Earth Science, 7*, 9. Retrieved from <Go to ISI>://WOS:000495416500001. doi:10.3389/feart.2019.00276

Yuan, B. X., Xu, K., Wang, Y. X., Chen, R., & Luo, Q. Z. (2017). Investigation of Deflection of a Laterally Loaded Pile and Soil Deformation Using the PIV Technique. *International Journal of Geomechanics, 17*(6), 9. Retrieved from <Go to ISI>://WOS:000399425700024. doi:10.1061/(asce)gm.1943-5622.0000842

Zheng, X. Y., Ying, Z., Wang, B., & Chen, C. (2018). Hydrogen and syngas production

from municipal solid waste (MSW) gasification via reusing CO2. *Applied Thermal Engineering, 144*, 242-247. Retrieved from <Go to ISI>://WOS:000451499600022. doi:10.1016/j.applthermaleng.2018.08.058

GB, Sample preparation and saturation, Standard for geotechnical testing method GB/T 50123-2019, 2019.

ASTM-International, Standard Test Method for Determination of the Impact Value (IV) of a Soil, ASTM D 5874-2015, 2015.